PAPER • OPEN ACCESS

Extended analytical solutions of the Bohr Hamiltonian with the sextic oscillator: Pt-Os isotopes

View the article online for updates and enhancements.

Extended analytical solutions of the Bohr Hamiltonian with the sextic oscillator: Pt-Os isotopes

S Baid[1,2] , G Lévai[3,*] and J M Arias[2,4]

[1] LPHEA, Faculty of Sciences Semlalia, Cadi Ayyad University, Morocco
[2] Departamento de FAMN. Facultad de Física, Universidad de Sevilla, 41080 Sevilla, Spain
[3] Institute for Nuclear Research (ATOMKI), PO Box 51, H-4001 Debrecen, Hungary
[4] Instituto Carlos I de FTC, Universidad de Granada, 18071 Granada, Spain

E-mail: sbaid@us.es, levai@atomki.hu and ariasc@us.es

CrossMark

Abstract

The sextic oscillator adapted to the Bohr Hamiltonian has been used to describe even Pt and Os isotopes from $A = 188$ to 198 and $A = 186$ to 192, respectively. The purpose of this study was to investigate the possible transition from the γ-unstable to the spherical vibrator shape phases. In this setup the potential appearing in the Bohr Hamiltonian is independent from the γ shape variable, and the physical observables (energy eigenvalues, $B(E2)$) can be obtained in closed analytical form within the quasi-exactly solvable formalism for the model space containing 30 of the lowest-lying levels. Experimental energy levels have been associated with the theoretical ones. The available electric quadrupole transition data ($B(E2)$, decay preferences) have been taken into account in matching the experimental and theoretical levels. Special attention has been paid to transitions from the first two excited 0^+ levels to the 2_1^+ and 2_2^+ levels, as these indicate the change of shape phases with spherical and deformed potential minimum. The three parameters of the Hamiltonian have been determined by a weighted least square fit procedure. Trends in the location of states belonging to the ground-state, the $K^\pi = 2^+$ and two excited $K^\pi = 0^+$ bands have been analysed. The trajectory determined by the fitted parameters in the two-dimensional phase space has also been plotted,

---

* Author to whom any correspondence should be addressed.

and it has been found that all the nuclei are characterized by a deformed potential minimum, except for the heaviest Pt isotope (^{198}Pt), for which the transition to the spherical shape phase is realised. Although the spectroscopic information on the next isotopes of the chains (^{200}Pt and ^{194}Os) is far less complete, there are indications that these nuclei are also close to or fall within the domain of spherical potential minimum.

(Some figures may appear in colour only in the online journal)

1. Introduction

The nucleus is a strongly interacting many-fermion system. Its dynamics are thus, governed by the nuclear forces and the Pauli exclusion principle. For the theoretical description of this system, a variety of models has been introduced, each focusing on different aspects. Single-particle models (like the shell model) describe the nucleus from the point of view of nucleons that move in the average potential generated by the other nucleons. Collective models capture the dynamics of the nucleus in terms of excitations of the nucleus as a whole. One of the most important feature of nuclei is their shape. Its description is carried out in different ways in the individual nuclear models. In the shell model, one can start from a spherical average potential, in which case the nuclear deformation develops due to the occupation of orbits by the protons and neutrons, or, alternatively, the average potential can be chosen non-spherical, which is reflected also in the deformation of the nucleus. In collective nuclear structure models the nuclear shape is considered as an input, and the nuclear excitations are interpreted as oscillations around the equilibrium nuclear shape. The shape associated with the ground-state configuration of the nucleus can be estimated from the location of the nucleus on the chart of nuclides, i.e. from its relative position from closed shells. The equilibrium nuclear shape can change along trajectories of the chart of nuclides, e.g. along isotope chains, so the description of the transition from one shape phase to another one is a notable challenge for all nuclear models.

The Bohr Hamiltonian has been developed to describe the quadrupole type excitations of nuclei [1–3]. The key variables are $\beta \geqslant 0$ measuring the deviation from the spherical shape and $\gamma \in [0, \pi/3]$ characterizing the deviation from the axially symmetric shape. The orientation of the nucleus is described by the Euler angles, so the problem is defined in a five-dimensional space. The kinetic term depends on all five variables, while the potential is the function of the intrinsic β and γ shape variables. The location of the potential minimum defines the nuclear shape: spherical, deformed prolate, deformed oblate, deformed triaxial, etc.

An important advance was the introduction of the Interacting Boson Model [4], in which quadrupole nuclear excitations are handled in terms of quadrupole (d) and monopole (s) bosons. The physical operators are constructed from boson-creating and annihilating operators such that the total number of bosons is conserved and the operator exhibits appropriate spherical tensorial ($O(3)$) character. The model has $U(6)$ group structure, furthermore, it has three limiting symmetries (subgroup chains), each associated with a characteristic nuclear shape: $U(5)$ for a spherical vibrator, $O(6)$ for deformed γ-unstable and $SU(3)$ for axially

deformed rotational nuclei. These symmetries helped the consistent interpretation of observables in a wide range of nuclei. The connection between the IBM Hamiltonian and the Bohr Hamiltonian has also been established [5, 6].

A further development was the study of quantum phase transitions in the transitional path from one nuclear shape phase to another. The existence of a second-order phase transition was established between the $U(5)$ (spherical) and the $O(6)$ (deformed γ-unstable) limits, and a first-order one between the $U(5)$ (spherical) and $SU(3)$ (axially deformed) limits [7]. Based on these results, symmetries associated with the critical points of shape transitions were introduced within the Bohr Hamiltonian scheme. Firstly, the $E(5)$ critical point symmetry was proposed for transitions from the spherical vibrator and the γ-unstable phases [8]. In this model, the $V(\beta, \gamma)$ potential of the Bohr Hamiltonian is approximated by the infinite square well in the β variable (the γ variable does not play any role here), which has analytical solutions in terms of Bessel functions. The flat potential shape for the β variable approximates the situation when the potential minimum $V(\beta = 0)$, associated with the spherical equilibrium shape of the anharmonic vibrator, develops gently through another situation in which a deformed potential minimum $V(\beta > 0)$, associated with the γ-unstable shape, appears without coexistence. The next proposed critical point symmetry was the $X(5)$ [9] occurring during the transition from the spherical vibrator to the axially deformed rotor phase. In this case, the γ shape variable also plays a role, so the formalism becomes more involved, but remains analytically solvable. In this case, the potential energy surface evolves as follows: starting from a spherical minimum, a second minimum higher in energy develops, this minimum goes down in energy until degeneration with the spherical minimum (critical point and shape coexistence) and continues going down in energy to be the lowest minimum. Equivalent critical points have been studied within the IBM scheme (for a nice review see [10]).

The introduction of the critical point symmetries triggered a search for nuclei that correspond to the predictions of these models, and also initiated the exploration of potentials that lead to exact solutions in the Bohr Hamiltonian (for a review see [11]). We contributed to these efforts by proposing the sextic oscillator as a potential in the β shape variable [12]. This potential has a flexible shape: depending on the parameters, it can have a spherical minimum, a deformed minimum or both, and the transition between these shape phases can be controlled analytically. It belongs to the class of quasi-exactly solvable (QES) potentials [13, 14] meaning that only the lowest few energy levels can be obtained exactly. The electromagnetic transition rates ($B(E2)$, $B(E0)$) have also been determined in closed form, and benchmark numbers associated with the transition between the shape phases have been calculated [15]. More recently, the range of QES solutions has been extended to wave functions with up to two nodes (previously solutions with up to one node had been considered): this development extended the number of levels to 30, with $L^{\pi} \leqslant 10$ [16]. A systematic description of Ru and Pd isotopes was presented and nuclei close to the transition from the spherical to deformed potential minimum were identified (^{104}Ru, ^{108}Pd).

The sextic oscillator has also been used in the Bohr Hamiltonian with potentials depending on the γ shape variable too. Various nuclear shapes have been considered: γ-stable triaxial [17], γ-stable prolate [18], γ-rigid triaxial [19] and γ-rigid prolate [20] nuclei (see [21] for a review). Numerical studies for the sextic oscillator have also been carried out to describe double-well structures [22]. The performance of higher QES solutions of the sextic oscillator has also been studied [23]. Here the solutions had to be determined by numerical diagonalization. The conclusion was that solutions up to two nodes seem to be the best approximation for phase transition studies.

In the present work, we apply the extended sextic oscillator potential QES model to another region of the nuclide chart, where transition between the spherical vibrator and the γ-unstable shape phases can be expected. This is the chain of even Pt and Os isotopes, located close to the closure of the $Z = 82$ proton shell. Some Pt nuclei have been considered the best examples for $O(6)$ symmetry [24], so it seems worthwhile to study the evolution of the spectroscopic properties along the named isotope chains. Recently, other theoretical works investigate the same region solving the Bohr equation considering energy-dependent parameters and/or deformation-dependent mass [25–28].

The paper is arranged as follows. The essential elements of the sextic oscillator adapted to the Bohr Hamiltonian are presented in section 2. In section 3 the experimental levels of Pt and Os nuclei are associated to model states, the model parameters are fitted and the findings are interpreted, while section 4 summarizes the results.

2. Review of the model

2.1. The Bohr Hamiltonian

The original Bohr collective Hamiltonian is given in terms of five curvilinear coordinates, including the intrinsic deformation variables β, γ, and the three Euler angles $(\theta_1, \theta_2, \theta_3)$. After separating the angular variables, it is written as follows [1, 2]:

$$H = -\frac{\hbar^2}{2B}\left[\frac{1}{\beta^4}\frac{\partial}{\partial\beta}\beta^4\frac{\partial}{\partial\beta} + \frac{1}{\beta^2\sin 3\gamma}\frac{\partial}{\partial\gamma}\sin 3\gamma\frac{\partial}{\partial\gamma} \right.$$

$$\left. -\frac{1}{4\beta^2}\sum_k \frac{Q_k^2}{\sin^2\left(\gamma - \frac{2}{3}\pi k\right)} \right] + V(\beta, \gamma), \tag{1}$$

where B is the mass parameter and $Q_k(k = 1, 2, 3)$ are the components of the angular momentum in the intrinsic reference frame. Here we consider the special case of γ-unstable potentials, which depend explicitly only on the β variable, i.e. $V(\beta, \gamma) = U(\beta)$. For these potentials the β-dependence can be separated into an equation similar to the radial Schrödinger equation by using the substitution

$$\Psi(\beta, \gamma, \theta_i) = \beta^{-2}\phi(\beta)\Phi(\gamma, \theta_i). \tag{2}$$

The β-differential equation is then

$$-\frac{\mathrm{d}^2\phi(\beta)}{\mathrm{d}\beta^2} + \left[\frac{(\tau + 1)(\tau + 2)}{\beta^2} + u(\beta) \right]\phi(\beta) = \epsilon\phi(\beta). \tag{3}$$

Here τ is the seniority quantum number, which determines the allowed L angular momentum values (see later). The reduced energies and potentials are defined as $\epsilon = \frac{2B}{\hbar^2}E$ and $u(\beta) = \frac{2B}{\hbar^2}U(\beta)$, respectively. Note that the deformation variable β is dimensionless, and so are $u(\beta)$ and ϵ. The mass parameter B has physical dimension kg m^2 and its chosen value sets the energy scale.

2.2. The sextic oscillator potential adapted to the Bohr Hamiltonian

Similarly to [12, 15, 16], we chose the potential $u(\beta)$ as the sextic oscillator, which is a member of the QES potential family [13]. A characteristic feature of these potentials is that

only their lowest few bound-state solutions can be obtained in closed analytical form. In general, their solutions are written in terms of an infinite power series, which can be reduced to an Mth order polynomial form for certain combination of the parameters appearing in the formulas. In the case of the sextic oscillator the coefficients of the power series are obtained from a three-term recurrence relation. This can be terminated by a suitable choice of the parameters, in which case the coefficients of the polynomial solutions are obtained by finding the roots of an $(M + 1)$th order algebraic equation. In general, the roots have to be calculated numerically, however, up to $M = 2$ (i.e. the cubic algebraic equation) they can be determined in closed form. It has to be noted that the conditions for the termination of the power series imply constraints on the potential parameters, so the QES solutions can be obtained only for special subsets of the general sextic oscillator. It may also be noted that the QES solutions of the sextic oscillator can also be obtained by a suitable transformation from the bi-confluent Heun equation: see [29] on the relation of the two approaches.

Here we review the essential ingredients of our model; any further details can be found in [12, 15, 16]. The polynomial QES solutions of the sextic oscillator can be written in the form

$$\phi(\beta) \sim \beta^{\tau+2} \exp\left[-\frac{a}{4}\beta^4 - \frac{b}{2}\beta^2 \right] P^{(M)}(\beta^2), \tag{4}$$

where $P^{(M)}(\beta^2)$ is an Mth order polynomial in β^2. Note that since β is dimensionless, so are a and b. Note also that normalizable solutions can only be obtained for $a \geqslant 0$. Substituting equation (4) into equation (3) one finds that the form of the sextic potential used in the Bohr Hamiltonian is [12, 15, 16]

$$u(\beta) = (b^2 - 4ac^\pi)\beta^2 + 2ab\beta^4 + a^2\beta^6 + u_0^\pi, \tag{5}$$

where a and b are real parameters appearing in the exponential factor of equation (4), while c^π is a constant that is determined by τ and M as

$$2c^\pi = \tau + 2M + \frac{7}{2}. \tag{6}$$

The u_0^π constants (defined later on) are used to match the τ-even and τ-odd parts of the spectrum: see [16] for the details on the calculations. Note that the $a = 0$ choice recovers the harmonic oscillator.

The shape of the potential equation (5) is determined by the signs of the coefficient of the quadratic, quartic and sextic terms The latter, a^2 is always positive, so the potential increases infinitely with increasing β. The sign of the coefficient of the quadratic term determines the potential close to the origin. For $b^2 > 4ac^\pi$, the potential has a local minimum at $\beta = 0$, while for $b^2 < 4ac^\pi$ it has a local maximum. For $b^2 = 4ac^\pi$ the quadratic term vanishes, so the potential is flat near the origin, and the coefficient of the quartic term determines what kind of extremum it has there. This coefficient, $2ab$, has the same sign as b. In other words, the (a, b) parameter space of the model is divided by the parabola $a = b^2/(4c^\pi)$ into three domains: I. Above the parabola the potential has a local maximum at the origin, and has a minimum for $\beta > 0$, irrespective of the sign of b; II. Below the parabola and for $b > 0$ all the coefficients are positive, so the potential has only a minimum at the origin. (for $a = 0$ the potential reduces to the harmonic oscillator); III. Below the parabola and for $b < 0$ the potential has a local minimum at the origin, another minimum at $\beta > 0$ and a local maximum in between. It can be proven that the minimum at $\beta > 0$ is always deeper [16]. Equation (6) implies that for $a > 0$, c^π is different for even and odd values of τ. This also means that the potential is slightly different for states with even and odd value of τ. The difference appears in the coefficient of the quadratic term in β, i.e. close to the origin and it is not too significant in general. This

duality of the potential in the parity of τ is similar to parity-dependent potentials, which are used in various branches of physics. However, it raises the question of how to adjust the two spectra to each other. In [12, 15, 16] this problem was handled by introducing the u_0^π constant in the potential equation (4). In particular, the minima of the two potentials were prescribed to coincide. This can be reached by the following choice of the u_0^+ and u_0^- used in the τ-even and τ-odd potential forms, respectively:

$$u_0^+ = 0, \tag{7}$$

$$
u_0^- =
\begin{cases}
(b^2 - 15a)(\beta_0^+)^2 - (b^2 - 17a)(\beta_0^-)^2 & \\
+2ab[(\beta_0^+)^4 - (\beta_0^-)^4] + a^2[(\beta_0^+)^6 - (\beta_0^-)^6]; & \text{if } b < (15a)^{\frac{1}{2}} \\
-(b^2 - 17a)(\beta_0^-)^2 - 2ab(\beta_0^-)^4 - a^2(\beta_0^+)^6; & \text{if } (15a)^{\frac{1}{2}} < b < (17a)^{\frac{1}{2}} \\
0; & \text{if } b > (17a)^{\frac{1}{2}}
\end{cases}, \tag{8}
$$

where

$$\beta_0^\pi = \frac{1}{3a}[-2b \pm (b^2 + 12ac^\pi)^{\frac{1}{2}}]. \tag{9}$$

See [12, 15, 16] for the detailed calculations.

In the first applications of the sextic oscillator in the Bohr Hamiltonian [12, 15] solutions with $M = 0$ and 1 were considered, while the extension up to $M = 2$ was worked out in [16]. This required the determination of the roots of a cubic algebraic equation in closed form. The normalised solutions are written as

$$\phi_\alpha(\beta) = N_\alpha \beta^{\tau+2}(1 + d_\alpha \beta^2 + g_\alpha \beta^4)\exp\left[-\frac{a}{4}\beta^4 - \frac{b}{2}\beta^2\right]. \tag{10}$$

Here α represents the quantum numbers (ξ, τ). $\xi = 1$, 2, and 3 is the traditional notation referring to the number of nodes n of the β-wave function as $\xi = n + 1$. The coefficients d_α and g_α can be determined in the knowledge of the roots of the cubic algebraic equation, while the normalization constants N_α can be calculated exactly in terms of confluent hypergeometric functions [12, 16].

The energy eigenvalues are determined for τ-even and τ-odd states separately. According to equation (6), the $\tau + 2M = 4$ choice that allows the combinations $\tau = 0$, $M = 2$; $\tau = 2$, $M = 1$ and $\tau = 4$, $M = 0$ corresponds to $c^+ = 15/4$, while $\tau + 2M = 5$ includes the combinations $\tau = 1$, $M = 2$; $\tau = 3$, $M = 1$ and $\tau = 5$, $M = 0$ corresponding to $c^- = 17/4$ [12] (this difference in c^+ and c^- also defines the difference of the τ-even and τ-odd potentials as $2a\beta^2$). The energy eigenvalues are displayed in table 1. The various $\lambda_i^{(M)}$ quantities appearing there are obtained from solution of the $(M + 1)$th order algebraic equations.

Introducing $s = (2\tau + 5)/4$, the quantities appearing in table 1 are as follows [16]:

$$
\begin{aligned}
\lambda_\pm^{(1)} &= 2b \pm 2(b^2 + 18a)^{\frac{1}{2}}, \\
\widetilde{\lambda}_\pm^{(1)} &= 2b \pm 2(b^2 + 22a)^{\frac{1}{2}},
\end{aligned}
\tag{11}
$$

Table 1. The energy eigenvalues of the sextic oscillator adapted to the Bohr Hamiltonian [16]. The constant terms u_0^π in equations (7) and (8) that depend on the even or odd value of τ are subtracted for simplicity. The $\lambda_i^{(M)}$ and $\tilde{\lambda}_i^{(M)}$ quantities are displayed in equations (11) and (12). The fifth column displays the angular momenta L contained in the given (ξ, τ) multiplet.

ξ	τ	M	$\epsilon_{\xi,\tau} - u_0^\pi$	L
1	0	2	$\begin{cases}\lambda_2^{(2)}; & b > 0, \\ \lambda_1^{(2)}; & b < 0,\end{cases}$	0
1	2	1	$9b + \lambda_-^{(1)}$	2, 4
1	4	0	$5b + \lambda_3^{(2)}$	2, 4, 5, 6, 8
2	0	2	$5b + \lambda_3^{(2)}$	0
2	2	1	$9b + \lambda_+^{(1)}$	2, 4
3	0	2	$5b + \begin{cases}\lambda_1^{(2)}; & b > 0, \\ \lambda_2^{(2)}; & b < 0,\end{cases}$	0
1	1	2	$7b + \begin{cases}\tilde{\lambda}_2^{(2)}; & b > 0, \\ \tilde{\lambda}_1^{(2)}; & b < 0,\end{cases}$	2
1	3	1	$11b + \tilde{\lambda}_-^{(1)}$	0, 3, 4, 6
1	5	0	$15b$	2, 4, 5, 6, 7, 8, 10
2	1	2	$7b + \tilde{\lambda}_3^{(2)}$	2
2	3	1	$11b + \tilde{\lambda}_+^{(1)}$	0, 3, 4, 6
3	1	2	$7b + \begin{cases}\tilde{\lambda}_1^{(2)}; & b > 0, \\ \tilde{\lambda}_2^{(2)}; & b < 0,\end{cases}$	2

$$\lambda_i^{(2)} = \Lambda_i^{(2)}(5/4), \quad s = 5/4 \quad \text{for } \tau = 0$$
$$\tilde{\lambda}_i^{(2)} = \Lambda_i^{(2)}(7/4), \quad s = 7/4 \quad \text{for } \tau = 1, \tag{12}$$

where

$$\Lambda_1^{(2)}(s) = 4b - 2r\cos\left(\frac{\phi}{3}\right),$$
$$\Lambda_2^{(2)}(s) = 4b + 2r\cos\left(\frac{\pi}{3} - \frac{\phi}{3}\right),$$
$$\Lambda_3^{(2)}(s) = 4b + 2r\cos\left(\frac{\pi}{3} + \frac{\phi}{3}\right),$$
$$\cos(\phi) = -\frac{64ab}{r^3},$$
$$r \equiv r(s) = \pm\left[\frac{16}{3}(b^2 + 2a(4s + 1))\right]^{\frac{1}{2}}, \tag{13}$$

and the prescription $\text{sgn}(r) = -\text{sgn}(b)$ has to be satisfied.

The (ξ, τ) multiplets contain one or more physical states with given L angular momentum value. The rules determining the allowed values follow from the $O(5) \supset O(3)$ decomposition: construct $\tau = 3n_\Delta + \nu$, with $n_\Delta = 0, 1, \ldots$. Then the allowed L-values are $L = \nu, \nu + 1, \ldots, 2\nu - 2, 2\nu$ (note that the value $L = 2\nu - 1$ is missing). Table 1 displays which L values are allowed for the given (ξ, τ) multiplets. In the original version of the model [12, 15], the states

belonging to the same multiplet were considered degenerate in energy. During the application of the extended model (up to $M = 2$) [12] it was found that the physical states do not follow this degeneracy, rather typically, the levels with higher L appear higher in the spectrum. For this reason, in [16] the Hamiltonian was extended by a phenomenological rotational term $cL \cdot L$. The justification of this rotational term has been presented in [12], referring to certain algebraic models of nuclear structure. The Casimir invariants of algebras associated to these models, e.g. the IBM are typically written as the sum of scalar products of the type $A^{(j)} \cdot A^{(j)}$. The most well-known example is the $SU(3)$ algebra, in which case the Casimir invariant is expressed in terms of the $L \cdot L$ and the $Q \cdot Q$ terms corresponding to $j = 1$ and $j = 2$, respectively. Introducing the physically relevant quadrupole–quadrupole interaction naturally introduces a rotational splitting in the spectrum. In the case of $O(6)$ and $O(5)$ algebras, which play an important role in the present model, the $L \cdot L$ term also appears in the Casimir operators together with other scalar products of the type $A^{(j)} \cdot A^{(j)}$ [4], so a rotational splitting can appear naturally. With the rotational term, the number of the model parameters increased to three: a, b and c.

In what follows, the energy scale will be redefined such that $E = 0$ corresponds to the ground-state energy. The rescaled energy eigenvalues will be denoted as

$$E_{\xi,\tau} = \epsilon_{\xi,\tau} - \epsilon_{1,0} . \tag{14}$$

The electric quadrupole transitions are calculated using the first-order transition operator [3, 8, 30]

$$T^{(E2)} = t\beta \left[D^{(2)}_{\mu,0}(\theta_i)\cos\gamma + \frac{1}{\sqrt{2}}(D^{(2)}_{\mu,2}(\theta_i) + D^{(2)}_{\mu,-2}(\theta_i))\sin\gamma \right]. \tag{15}$$

The integrals in β necessary for its matrix elements can be calculated exactly in terms of confluent hypergeometric functions [16]. This first-order transition operator leads to selection rules $\Delta\tau = \pm 1$, which also means that the matrix elements for the electric quadrupole moments vanish. This selection rule can be relaxed by adding a second-order term to (15):

$$T^{(E2)'} = T^{(E2)} + t'\beta^2 \left[-D^{(2)}_{\mu,0}(\theta_i)\cos(2\gamma) + \frac{1}{\sqrt{2}}(D^{(2)}_{\mu,2}(\theta_i) + D^{(2)}_{\mu,-2}(\theta_i))\sin(2\gamma) \right]. \tag{16}$$

Note that the first-order operator in equation (15) is an $O(6)$ generator, so implies strict selection rules for τ, which is an $O(5)$ quantum number. In contrast to this, the second-order transition operator (16) is no more an $O(6)$ generator, so transitions with $\Delta\tau = 0, \pm 1, \pm 2$ are allowed. It should be noted that the Jacobian in the (β, γ) intrinsic variables is $\beta^4 |\sin(3\gamma)|$.

3. Application for Pt and Os isotopes

In a previous study [16], the model was applied to even-mass Ru and Pd nuclei, which are located near the closure of the $Z = 50$ shell. In analogy with that work, here nuclei near the closure of the $Z = 82$ shell are discussed: the chain of even-mass Pt ($A = 188$ to 198) and Os ($A = 186$ to 192) isotopes. The heaviest Pt isotopes also approach the $N = 126$ shell closure. These regions are expected to accommodate nuclei with spherical vibrator and γ-unstable [30] character, and may present examples for the transition between these shape phases. The selection criterion was that the given isotope should have rich enough experimental spectrum up to about $E = 2500$ keV and $L^\pi = 10^+$. Data were taken from NNDC compilation.[5]

---

[5] http://www.nndc.bnl.gov/nndc/ensdf/.

All calculations have been done, as mentioned above, including in the Hamiltonian an extra term cL^2 so as to break the L-degeneracy within a τ multiplet:

$$H = -\frac{d^2\phi(\beta)}{d\beta^2} + \left[\frac{(\tau+1)(\tau+2)}{\beta^2} + u(\beta)\right] + cL \cdot L, \qquad (17)$$

where $u(\beta) = \frac{2B}{\hbar^2}U(\beta)$ is given by equation (5). Thus, one has three parameters: (a, b) defining the potential and c controlling the L-splitting. Using the reduced energy quantities, c is dimensionless, similar to a and b. In what follows, we set the energy scale such that $\hbar^2/(2B) = 1$ keV, i.e. $B = 500\hbar^2$ MeV^{-1}. With this choice, the physical energy values measured in keV coincide with the calculated dimensionless energy values.

3.1. State and band assignment

Model states were assigned to the experimental levels based on their energy and, if available, the $B(E2)$ values of their electric quadrupole transitions. The three model parameters (a, b and c) were fitted to the experimental spectrum using a two-step procedure, which was also applied in [16]. In the first step the lowest two even-spin states, and the lowest odd-spin states were identified with model states. These were the $(\xi, \tau)L^\pi = (1, 3)0^+$, $(2, 0)0^+$, $(1, 1)2^+$, $(1, 2)2^+$, $(1, 2)4^+$, $(1, 3)4^+$, $(1, 3)6^+$, $(1, 4)6^+$, $(1, 4)8^+$, $(1, 5)8^+$, $(1, 5)10^+$, and the $(1, 3)3^+$, $(1, 4)5^+$, $(1, 5)7^+$ levels (note that there is only one 10^+ state in the model spectrum, while 1^+ and 9^+ states are missing). The relative order of the levels with the same L is unambiguous: states with higher τ are expected to lie higher. The only exception occurs for the $L^\pi = 0^+$ states. Here both $(\xi, \tau)L^\pi = (1, 3)0^+$ and $(2, 0)0^+$ states can be the first excited level, depending on the parameters. However, the electric quadrupole decays of the two states are different, which helps their assignment [16]. The $(1, 3)0^+$ level decays to the $(1, 2)2^+$ level, which is expected to be the second excited 2^+ state, while the $(2, 0)0^+$ level decays to the $(1, 1)2^+$ level, which is typically the first excited one.

This procedure was applied to the six Pt and four Os isotopes selected here. There were only a handful of levels for which no experimental candidate could be identified: the corresponding model states all belong to the $(1, 5)$ multiplet (one 8^+, one 10^+, and three 7^+ states). After this first round of the level assignment, the parameters were fitted to the experimental spectrum. Following the procedure applied in [16] various weights were used for the individual levels. In particular, in order to avoid the overrepresentation of less well-known higher-lying states, the weight of unity ($w = 1$) was distributed evenly among the levels belonging to the same (ξ, τ) multiplets. In particular, the members of the $(1, 2)$, $(1, 3)$, $(1, 4)$ and $(1, 5)$ multiplets carried the weight $1/2$, $1/4$, $1/5$ and $1/7$, respectively, while the states that stood alone in their multiplet (e.g. $(1, 1)2^+$, $(2, 0)0^+$, etc) had weight $w = 1$. Furthermore, when the experimental spin-parity of the level was ambiguous, then the corresponding weight was halved.

As discussed previously, the bandhead state of the first two excited $K^\pi = 0^+$ bands can be assigned either to the $(1, 3)$ or the $(2, 0)$ quantum numbers. Experimental data for the $B(E2)$ values for the transitions from the second and third 0^+ states to the first two 2^+ states is displayed in table 2. It is seen that the 0_2^+ state prefers decaying to the 2_2^+ state in most cases. Relatively strong transitions have been observed for ^{194}Pt, ^{196}Pt, ^{190}Os and ^{192}Os. The $B(E2)$ value is smaller for ^{188}Os, but the preference holds in that case too. In terms of the model, this indicates that the 0_2^+ states can be assigned to the model state with $(\xi, \tau) = (1, 3)$. Based on the position of the first excited 0^+ state, the same assignment seems reasonable for the remaining nuclei, with the exception of ^{198}Pt. In this case, this state prefers decaying into the first excited 2^+ level, which supports its assignment to the model state with quantum numbers $(2, 0)0^+$.

Table 2. E2 transitions from the first two excited 0^+ states to the first two 2^+ states. Whenever the $B(E2)$ value is known, its relative strength to $B(E2; 2_1^+ \rightarrow 0_1^+)$ is displayed as $R_{ij} = B(E2; 0_i^+ \rightarrow 2_j^+)/B(E2; 2_1^+ \rightarrow 0_1^+)$, together with the corresponding error. The experimental data are from.[5] '+' indicates that the corresponding transition has been observed, but the $B(E2)$ value is not available.

| Nucleus | 0_2^+ state | | Decay to 2_1^+ | Decay to 2_2^+ | 0_3^+ state | | Decay to 2_1^+ | Decay to 2_2^+ |
	E_{exp} (keV)	L^π	R_{21}	R_{22}	E_{exp} (keV)	L^π	R_{31}	R_{32}
^{188}Pt	799	0^+	+	+	1674	$(0^+, 1, 2)$	+	
^{190}Pt	921	0^+	+	+	1670	0^+		
^{192}Pt	1195	0^+	+	+	1629	0^+	+	+
^{194}Pt	1267	0^+	0.013(3)	0.170(39)	1547	0^+	0.289(212)	0.291(223)
^{196}Pt	1135	0^+	0.069(37)	0.443(246)	1403	0^+	<0.123	<0.010
^{198}Pt	915	0^+	0.817(220)		1481	0^+	+	
^{186}Os	1061	0^+	10^{-3}		1456	0^+		
^{188}Os	1086	0^+	0.012(1)	0.062(4)	1478	0^+	+	+
^{190}Os	911	0^+	0.033(8)	0.329(117)	1545	0^+	+	+
^{192}Os	956	0^+	0.009(2)	0.490(43)	1206	0^+	0.004(1)	

J. Phys. G: Nucl. Part. Phys. **50** (2023) 045104

S Baid *et al*

10

Data are more scarce for decays from the 0_3^+ state. There is no information for decays from this state in ^{190}Pt and ^{186}Os. Transition to the 2_1^+ state has been observed in the remaining eight nuclei, with three known $B(E2)$ values: one relatively strong (^{194}Pt) and two weak (^{196}Pt, ^{192}Os). Transitions to the 2_2^+ states have been observed only for five nuclei, with two known $B(E2)$ values. In the case of ^{196}Pt this transition is weak, while for ^{194}Pt its strength is comparable to that of the transition to the 2_1^+ state. All these findings seem to indicate that the 0_3^+ state can be interpreted as the $(\xi, \tau) = (2, 0)$ model state (with the exception of ^{198}Pt). It has to be noted that there are further 0^+ states in two nuclei below the 0_3^+ states mentioned here, but these seem to be disjoint from the states discussed here. There are decays to the 0^+ state at 1479 keV in ^{194}Pt only from 1^+ and 1^- states, which are missing from the present model. In ^{190}Os there is a state with tentative spin-parity assignment $(0, 1, 2)^+$ at 1382 keV, but there are no observed transitions to and from it. These two states were thus omitted from the analysis by assuming that they have different structure.

The parameters determined from the fitting procedure were used to calculate the energy of all the model states. In the second round of the fitting procedure further experimental levels were assigned to the model states based on their energy, spin-parity and electric quadrupole decays. In most cases numerical $B(E2)$ values were not available in the NNDC compilation,[5] however, information on which other levels the given level decays to was presented. Combining these with the selection rules of the model [16] allowed further level assignments using the prescriptions presented above. Further states with ambiguous spin-parity values differing from the model predictions were also considered with zero weight in case the observed spectroscopic information (energy, possible L^π and the observed electromagnetic transitions) were in accordance with the predicted characteristics of a model state. The lowest unassigned experimental state (typically 2_3^+) is located at 1200 to 1500 keV. The result of the second fitting procedure are presented in tables 3 and 4. Predicted theoretical states are those without experimental correspondents, as well as those associated with $E_{\exp}$ values that are printed in parenthesis and italics.

The weighted root mean square deviation D of the theoretical and experimental spectrum is in the range of 50–90 keV for Pt nuclei and 90 to 130 keV for Os nuclei. The latter is comparable to the D values found for the Ru and the Pd nuclei in [16], while the results for the Pt nuclei show better agreement between the experimental and theoretical spectra. The largest deviation occurs typically for the $(\xi, \tau)L^\pi = (1, 3)0^+$ states: for three Pt and three Os nuclei E_{th} underestimates $E_{\exp}$ by more than 200 keV. This may be due to the fact that the levels assigned to the $(1, 3)$ multiplet do not follow a rotational pattern, rather the $(1, 3)0^+$ member is often located above the other member levels. There are also two nuclei in both chains, for which the theoretical $(1, 4)5^+$ level comes out more than 200 keV above its experimental counterpart (there are altogether 7 and 6 levels for the Pt and Os nuclei, respectively, with such a large energy difference).

3.2. Comparison with experiment

The experimental energy levels can be arranged into a $K^\pi = 0^+$ ground-state band, a $K^\pi = 2^+$ band and two excited $K^\pi = 0^+$ bands. These states are essentially the same as those taken into account in the first round of fitting the model parameters (the model space contains further bands too, however, these appear in the spectrum at higher energies, so their identification with experimental states may rest on less firm grounds). Figures 1, 2 and 3 display the members of the ground-state band, those of the $K^\pi = 2^+$ band and those of the first two excited $K^\pi = 0^+$ bands for the Pt isotopes, respectively. The same plots for the Os isotopes are presented in figures 4, 5 and 6. The ground-state bands are complete, with the exception of ^{198}Pt, where there is no experimental candidate for the $(\xi, \tau)L^\pi = (1, 5)10^+$ level. There are

Table 3. The theoretical energy eigenvalues E_{th} for the Pt isotopes compared with the available experimental data E_{exp} (keV).[5,a] E_{exp} in parenthesis indicates uncertain L^π assignment. An asterisk in front of $(\xi, \tau)L^\pi$ signifies that the given level was considered in the first round of the fitting procedure. E_{exp} in parenthesis and italics stand for experimental levels with tentative L^π differing from that of the corresponding theoretical levels, but which could be identified with them based on the available spectroscopic data. These states were not included in the fitting procedure. The potential parameters a, b and c obtained from the second round of the fitting procedure are displayed in the last section of the table, followed by the weighted root mean square deviation D.

$(\xi, \tau)L^\pi$	^{188}Pt E_{exp}	E_{th}	^{190}Pt E_{exp}	E_{th}	^{192}Pt E_{exp}	E_{th}	^{194}Pt E_{exp}	E_{th}	^{196}Pt E_{exp}	E_{th}	^{198}Pt E_{exp}	E_{th}
*(1, 1)2+	265	282	296	292	316	308	328	323	355	328	407	404
*(1, 2)2+	605	536	598	559	612	605	622	645	688	629	775	860
*(1, 2)4+	671	627	737	661	785	706	811	758	876	796	985	987
*(1, 3)0+	798	873	921	899	1195	965	1267	1010	1135	941	1481	1178
*(1, 3)3+	936	952	916	986	921	1052	923	1107	1015	1084	(1248)	1288
*(1, 3)4+	1085	1004	(1128)	1045	1201	1110	1229	1172	1293	1180	(1286)	1361
*(1, 3)6+	(1184)	1147	1287	1206	1365	1270	(1412)	1349	1525	1443	(1714)	1561
(1, 4)2+	1312	1358	1395	1404	1439	1510	1512	1587	1361	1506	(1550)	1745
(1, 4)4+	—	1449	(1385)	1507	1666	1611	*(1592)*	1700	1536	1674	(1748)	1873
*(1, 4)5+	—	1515	(1450)	1580	1482	1684	*(1498)*	1781	(1610)	1793	—	1964
*(1, 4)6+	1636	1593	(1732)	1668	1869	1771	(1926)	1878	2007	1937	1943	2073
*(1, 4)8+	1782	1788	1915	1887	2018	1988	(2100)	2121	2252	2295	(2527)	2347
(1, 5)2+	(1810)	1837	—	1890	2073	2016	(2214)	2100	(1984)	1982	(2120)	2138
(1, 5)4+	—	1928	—	1992	(1934)	2118	(2248)	2213	(2087)	2149	(2155)	2266
(1, 5)5+	—	1993	—	2065	—	2190	*(2356)*	2294	(2244)	2269	—	2357
(1, 5)6+	—	2072	—	2153	—	2277	(2569)	2391	—	2412	—	2466
*(1, 5)7+	—	2163	*(2043)*	2256	2113	2379	(2423)	2505	—	2580	—	2594
*(1, 5)8+	2246	2267	—	2373	2591	2495	2689	2634	(2750)	2771	2747	2739
*(1, 5)10+	2437	2515	2535	2650	2729	2770	(2917)	2941	(3044)	3225	—	3086
*(2, 0)0+	(1674)	1718	1670	1674	1629	1627	1547	1541	1403	1414	914	869
(2, 1)2+	(2295)	2223	(2216)	2193	2171	2171	(2158)	2102	(1968)	1962	1279	1319
(2, 2)2+	(2468)	2525	(2497)	2520	(2562)	2553	(2397)	2531	(2444)	2366	(1718)	1845
(2, 2)4+	—	2616	—	2622	—	2654	2640	2645	(2631)	2533	(2083)	1972
(2, 3)0+	*(2909)*	3067	—	3063	—	3118	(3132)	3095	(2659)	2862	—	2203

S Baid *et al*

Table 3. (Continued.)

$(\xi, \tau)L^{\pi}$	^{188}Pt E_{exp}	E_{th}	^{190}Pt E_{exp}	E_{th}	^{192}Pt E_{exp}	E_{th}	^{194}Pt E_{exp}	E_{th}	^{196}Pt E_{exp}	E_{th}	^{198}Pt E_{exp}	E_{th}
$(2, 3)3^+$	—	3145	—	3151	—	3205	—	3192	—	3005	*(2319)*	2312
$(2, 3)4^+$	—	3197	—	3210	—	3263	—	3257	—	3101	(2289)	2385
$(2, 3)6^+$	—	3341	—	3371	—	3423	—	3435	—	3364	—	2585
$(3, 0)0^+$	—	3272	—	3217	—	3185	(3065)	3081	—	2837	1869	1846
$(3, 1)2^+$	—	4039	—	3995	—	3983	—	3881	—	3603	(2356)	2333
a	13 332		13 105		13 116		12 357		10 477		1226	
b	−86.06		−67.53		−34.47		−0.47		4.36		196	
c	6.51		7.31		7.25		8.08		11.95		9.11	
$D(keV)$	53		52		89		88		87		88	

[a] https://www.nndc.bnl.gov/nudat3/.

J. Phys. G: Nucl. Part. Phys. **50** (2023) 045104

S Baid *et al*

Table 4. The same as table 3 for the Os isotopes.

$(\xi, \tau)L^{\pi}$	^{186}Os E_{exp}	E_{th}	^{188}Os E_{exp}	E_{th}	^{190}Os E_{exp}	E_{th}	^{192}Os E_{exp}	E_{th}
*$(1, 1)2^+$	137	242	155	247	187	247	206	235
*$(1, 2)2^+$	767	501	633	488	558	456	489	425
*$(1, 2)4^+$	434	536	478	534	548	556	580	559
*$(1, 3)0^+$	1061	830	1086	817	912	732	956	641
*$(1, 3)3^+$	910	860	790	856	756	818	690	756
*$(1, 3)4^+$	1070	880	966	883	955	875	909	833
*$(1, 3)6^+$	869	934	(940)	955	(1050)	1031	(1089)	1044
$(1, 4)2^+$	1208	1278	1305	1257	1114	1147	(1127)	1028
$(1, 4)4^+$	1352	1312	1279	1303	1163	1246	1069	1162
*$(1, 4)5^+$	1276	1337	1181	1335	1204	1317	1144	1258
*$(1, 4)6^+$	1491	1367	1425	1375	(1474)	1403	1465	1373
*$(1, 4)8^+$	1421	1441	1515	1473	1667	1616	1708	1661
$(1, 5)2^+$	(1653)	1707	1729	1698	(1689)	1553	(1409)	1374
$(1, 5)4^+$	(1704)	1741	*(1685)*	1744	(1708)	1653	(1456)	1508
$(1, 5)5^+$	(1775)	1766	1516	1777	(1446)	1724	(1362)	1604
$(1, 5)6^+$	(1813)	1796	—	1816	(1836)	1809	(1645)	1719
*$(1, 5)7^+$	(1751)	1831	1685	1862	*(2068)*	1909	1713	1853
*$(1, 5)8^+$	2015	(1870)	1980	1915	(2090)	2023	2134	2007
*$(1, 5)10^+$	2068	1965	2170	2039	(2358)	2293	(2419)	2371
*$(2, 0)0^+$	1456	1334	1478	1523	1545	1506	1206	1189
$(2, 1)2^+$	(1754)	1776	2124	1974	(1943)	1942	(1665)	1585
$(2, 2)2^+$	(1848)	2116	2204	2272	(2352)	2185	(1807)	1819
$(2, 2)4^+$	2081	2150	—	2317	(2124)	2284	(1780)	1954
$(2, 3)0^+$	—	2615	—	2786	(2563)	2636	(2147)	2180
$(2, 3)3^+$	—	2645	2622	2825	(2663)	2721	(2308)	2295
$(2, 3)4^+$	(2599)	2665	—	2851	—	2778	(2275)	2372
$(2, 3)6^+$	(2666)	2719	—	2924	—	2934	—	2583
$(3, 0)0^+$	—	2637	—	2926	(2820)	2849	—	2287
$(3, 1)2^+$	—	3287	—	3613	—	3513	—	2867
a	9041.7		10838		9950		6629	
b	−15.31		−61.47		−86.97		−47.04	
c	2.47		3.28		7.11		9.58	
D (keV)	132		113		86		97	

more missing experimental candidates in the $K^{\pi} = 2^+$ bands, and even more in the first two excited $K^{\pi} = 0^+$ bands. This is mainly due to the finding that the experimental spectra tend to be incomplete above 2200–2500 keV.

The members of the ground-state band are connected by strong E2 transitions (with the exception of the ^{190}Pt nucleus, for which only a single transition to the ground-state has been observed). This pattern is fairly well reproduced by the model spectrum, which contains the theoretical levels $(1, 0)0^+$, $(1, 1)2^+$, $(1, 2)4^+$, $(1, 3)6^+$, $(1, 4)8^+$ and $(1, 5)10^+$ (see figures 1 and 4).

The even-spin members of the $K^{\pi} = 2^+$ band are also characterized by strong E2 transitions in the case of the four Os nuclei, ^{194}Pt and ^{196}Pt. For these nuclei, relatively strong interband transitions have been observed to the ground-state band too. These experimental states can be identified as the $(1, 2)2^+$, $(1, 3)4^+$, $(1, 4)6^+$ and $(1, 5)8^+$ model states. There are relatively few $B(E2)$ data for transitions involving the odd-spin members of the $K^{\pi} = 2^+$
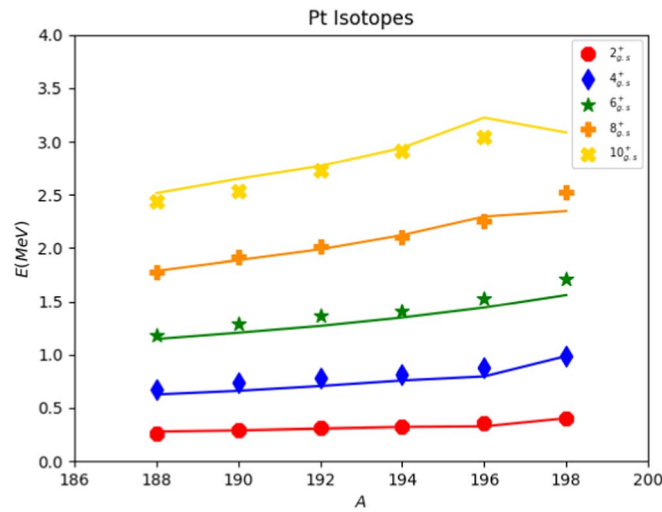
Figure 1. Members of the ground-state bands for Pt isotopes. Lines indicate the theoretical levels $(\xi, \tau)L = (1, 1)2$, $(1, 2)4$, $(1, 3)6$, $(1, 4)8$ and $(1, 5)10$, while the corresponding experimental states are represented by various symbols of the same colour. These are typically the lowest-lying energy levels for each L^{π}. The ground-state with $(\xi, \tau)L = (1, 0)0$ and $E = 0$ is not displayed.
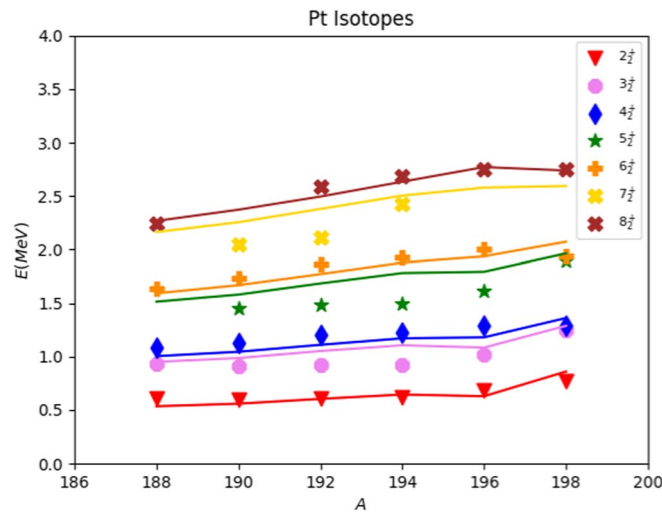

Figure 2. Members of the $K^{\pi} = 2^+$ bands for the Pt isotopes. Lines indicate the theoretical levels $(\xi, \tau)L = (1, 2)2$, $(1, 3)3$, $(1, 3)4$, $(1, 4)5$, $(1, 4)6$, $(1, 5)7$ and $(1, 5)8$, while the corresponding experimental states are represented by various symbols of the same colour. For even and odd-spin, these states are typically the second lowest and lowest-lying energy levels, respectively, for each L^{π}.

band, i.e. the lowest-lying 3^+, 5^+ and 7^+ levels. These states can be interpreted as the model states with the quantum numbers $(1, 3)3^+$, $(1, 4)5^+$ and $(1, 5)7^+$. The experimentally observed spacing of the $K^{\pi} = 2^+$ band is not always reproduced by the model: the odd-spin members usually predicted higher (see figures 2 and 5. This is because the splitting between
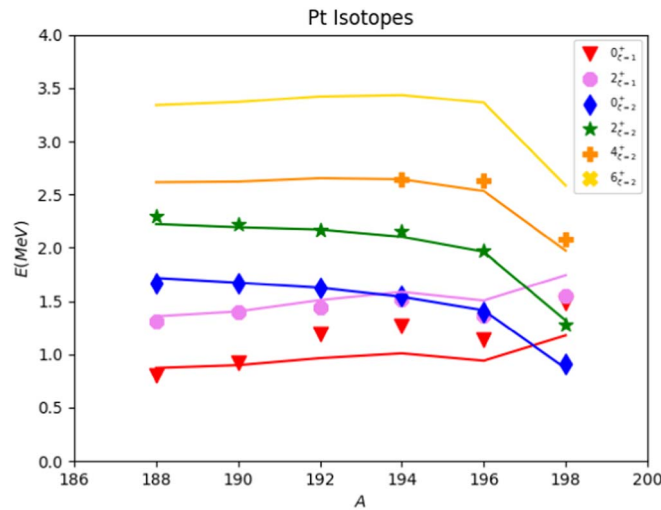
Figure 3. Members of the first two excited $K^\pi = 0^+$ bands for the Pt isotopes. Lines indicate the theoretical levels $(\xi, \tau)L = (1, 3)0, (1, 4)2$ for the first band, and $(2, 0)0, (2, 1)2, (2, 2)4$ and $(2,3)6$ for the second one, while the corresponding experimental states are represented by various symbols of the same colour. The indices $\xi = 1$ and $\xi = 2$ denote the two bands.
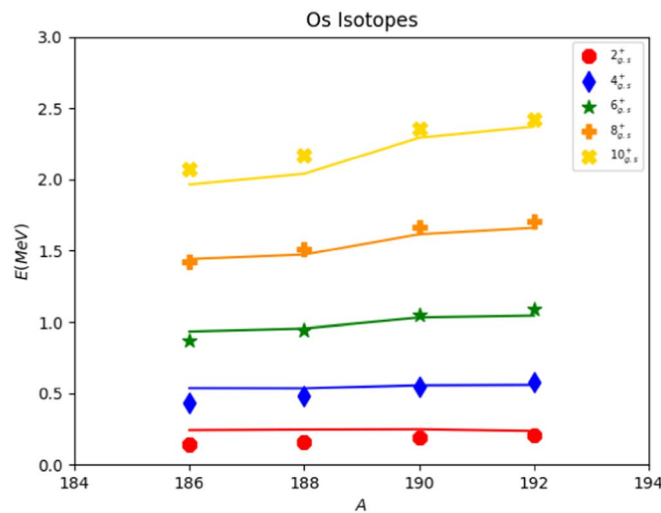
Figure 4. The same as figure 1 for the Os isotopes.

the pairs $[(1, 3)3^+, (1, 3)4^+], [(1, 4)5^+, (1, 4)6^+]$ and $[(1, 5)7^+, (1, 5)8^+)]$ is determined by the phenomenologic rotational term, $cL \cdot L$, the c parameter of which comes out relatively small from the fitting procedure. It has to be mentioned though, that the general structure of the $K^\pi = 2^+$ band is changing along the Pt chain, as it can be seen in figure 2. Starting from the light side of the chain, a typical rotational spacing can be observed for most nuclei. Then the splitting between the 2^+ and 3^+ states begins to increase, while that between the 3^+ and 4^+ states is shrinking, and for ^{198}Pt the latter two states form an almost degenerate doublet.

16
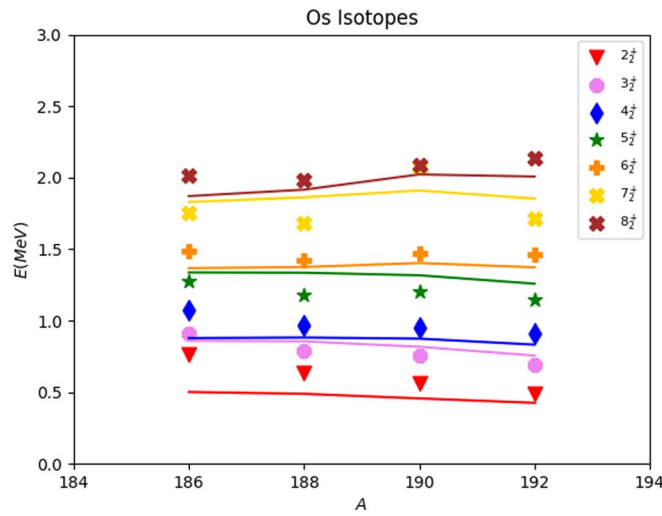
Figure 5. The same as figure 2 for the Os isotopes.
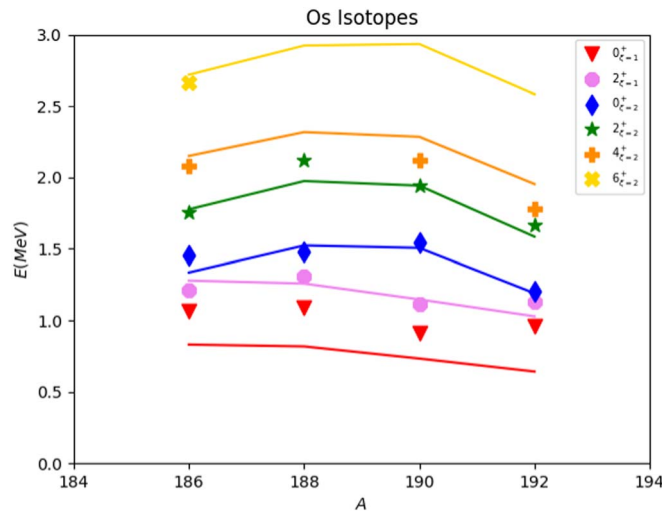
Figure 6. The same as figure 3 for the Os isotopes.

Similar trend is seen for the 5^+ members of this band and its neighbors. This trend is less visible in the Os chain (see figure 5).

It is seen in figures 3 and 6 that the members of the band built on the bandhead state identified with the $(2, 0)0^+$ model state exhibit a uniform decreasing trend in energy as the mass number is increasing, while the members of the bands built on the $(1, 3)0^+$ state stay roughly at the same energy throughout the chains. This leads to the phenomenon discussed before, i.e. that the $(2, 0)0^+$ state gets below the $(1, 3)0^+$ state in ^{198}Pt. This crossing does not occur in the Os chain, although the two 0^+ bandhead states get close to each other in ^{192}Os. Figures 7–13 present the most well-known part of the spectra, together with the available $B(E2)$ values given in W.u. The theoretical calculations have been done using the linear

17
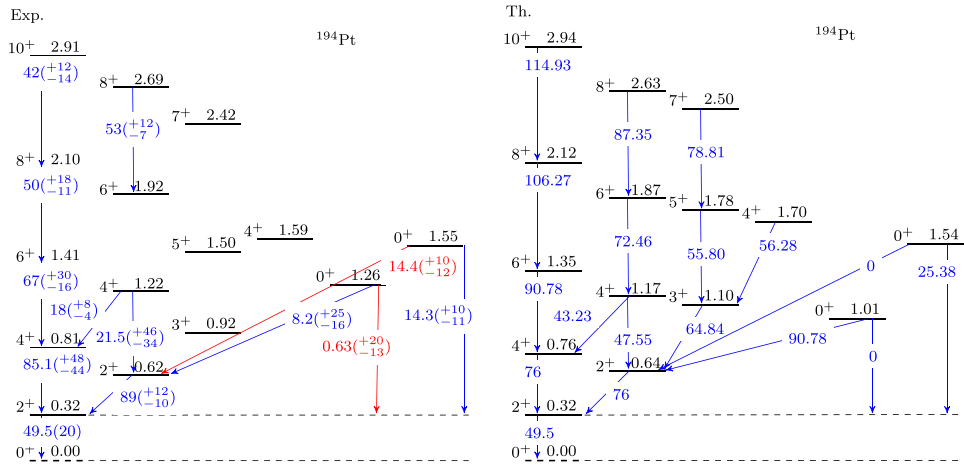
Figure 7. The experimental and theoretical energy (in MeV) spectrum of ^{194}Pt with the E2 transitions. The linear E2 operator, equation (15), has been used with $t = 8.58$ e b, in order to match the transition $B(E2; 2^+_1 \rightarrow 0^+_1)$. Transitions predicted to be forbidden in the model are displayed in red in the experimental (left) panel. Two forbidden transitions with $B(E2) \leqslant 0.36$ W.u. were omitted for the sake of clarity.
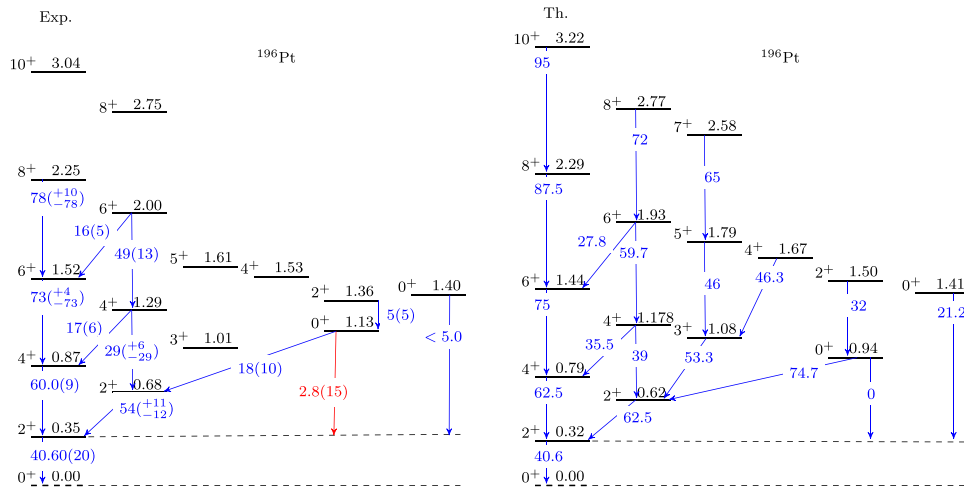
Figure 8. The same as figure 7 for ^{196}Pt. The linear E2 operator, equation (15), has been used with $t = 8.37$ e b, in order to match the transition $B(E2; 2^+_1 \rightarrow 0^+_1)$. Seven forbidden transitions with $B(E2) \leqslant 0.56$ W.u. were omitted for the sake of clarity.

quadrupole operator, equation (15). The parameter t in equation (15) was fixed to match the experimental $B(E2; 2^+_1 \rightarrow 0^+_1)$. A geometric estimate of the t parameter is $3ZR_0^2/(4\pi)$, where $R_0 = 1.2\,A^{1/3}$ fm. This estimated value is around 9 e b and 8.6 e b for the Pt and Os isotopes, respectively. Except for the two light Os isotopes, the estimated value is within 10 percent to the calculated one.

Table 5 summarizes the experimental information on the electric quadrupole transitions between states discussed here. There are only a few known $B(E2)$ values in the three light Pt
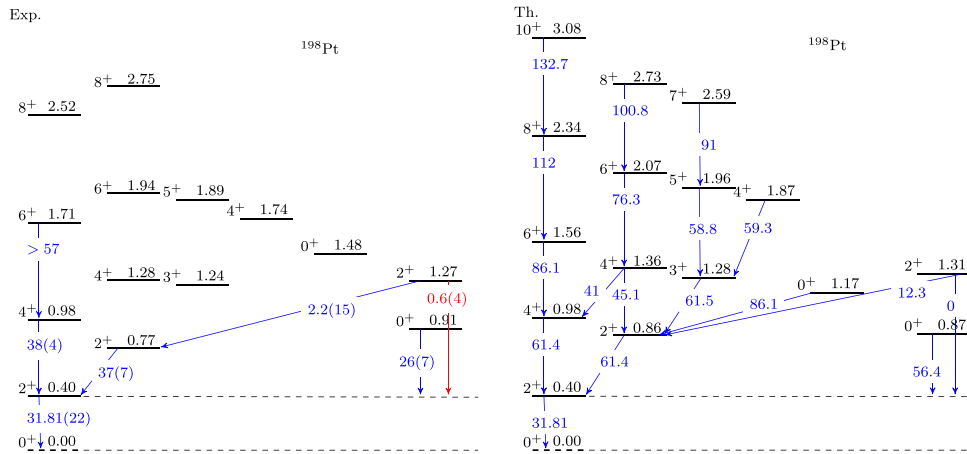
Figure 9. The same as figure 7 for ^{198}Pt. The linear E2 operator, equation (15), has been used with $t = 9.24$ e b, in order to match the transition $B(E2; 2_1^+ \rightarrow 0_1^+)$. Two forbidden transitions with $B(E2) \leqslant 0.05$ W.u. were omitted for the sake of clarity.
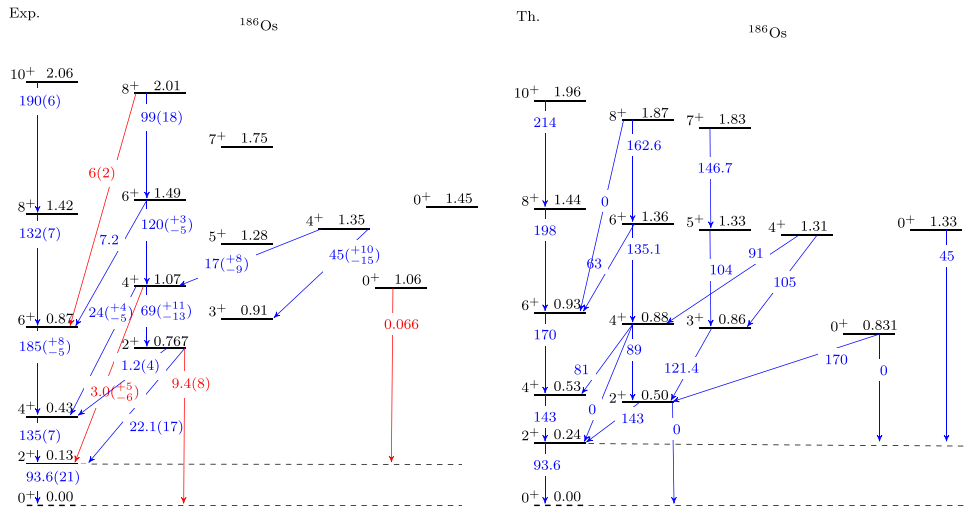

Figure 10. The same as figure 7 for ^{186}Os. The linear E2 operator, equation (15), has been used with $t = 11.48$ e b, in order to match the transition $B(E2; 2_1^+ \rightarrow 0_1^+)$. Two forbidden transitions with $B(E2) \leqslant 1.2$ W.u. were omitted for the sake of clarity.

isotopes, while the data set is more abundant in ^{194}Pt, ^{196}Pt and in the Os isotopes. It is reasonable to discuss separately the transitions with $\Delta\tau = \pm 1$ that are allowed using the linear E2 transition operator (15) and those that are forbidden. The average strength of the allowed transitions is typically one or two orders of magnitude larger. However, there are some relatively strong transitions with $\Delta\tau = \pm 2$ that the model predicts to be forbidden. This is the case for three of the four Os isotopes with the E2 transition from the 4_3^+ state to the 2_2^+ state. The strength of these transitions is in the range of 7–10 W.u., which reaches 10 to 17 percent of the strength of the transition from the 2_1^+ state to the ground-state in the given nucleus. In
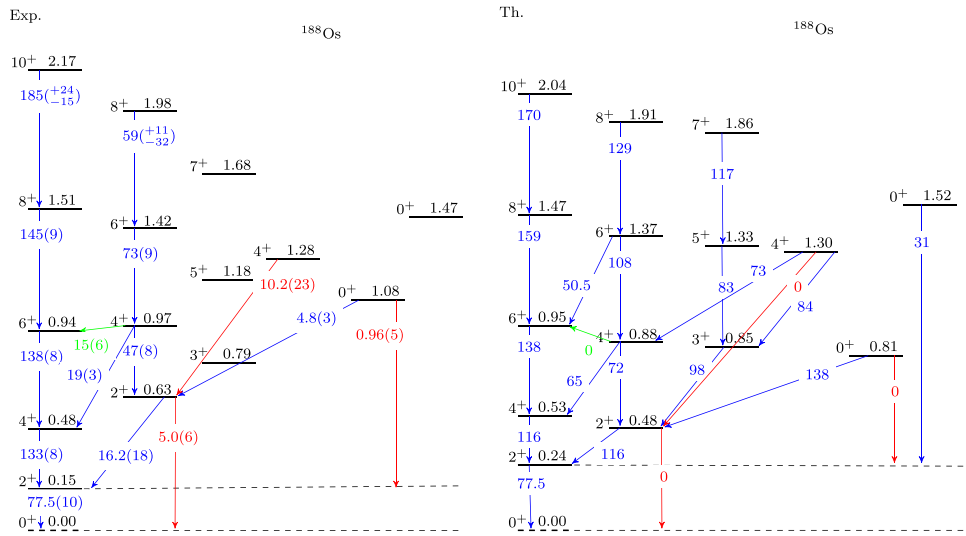
Figure 11. The same as figure 7 for ^{188}Os. The linear E2 operator, equation (15), has been used with $t = 10.35$ e b, in order to match the transition $B(E2; 2_1^+ \rightarrow 0_1^+)$. Three forbidden transitions with $B(E2) \leqslant 1.31$ W.u. were omitted for the sake of clarity. The transition indicated with green arrow occurs within the $(\xi, \tau) = (1, 3)$ multiplet and is forbidden due to the $\Delta\tau = 0$ selection rule.
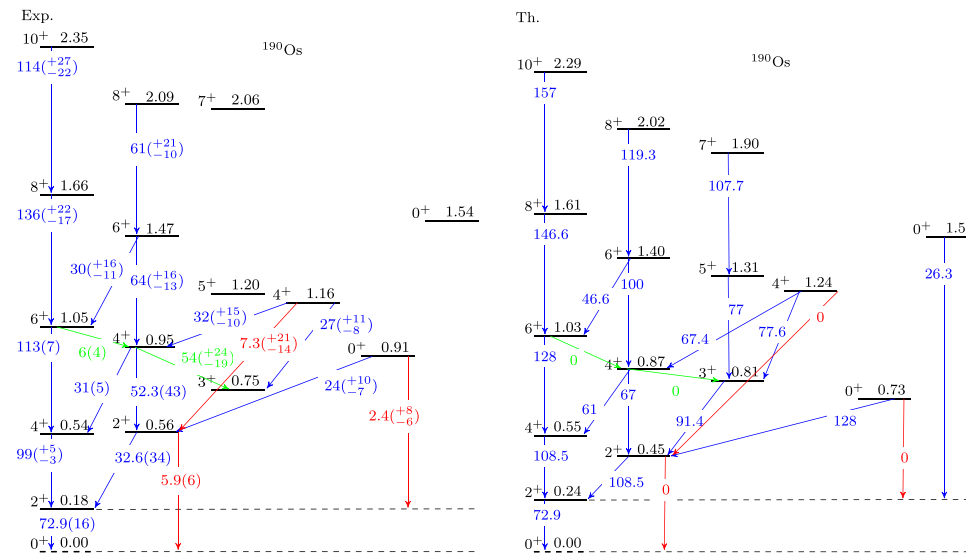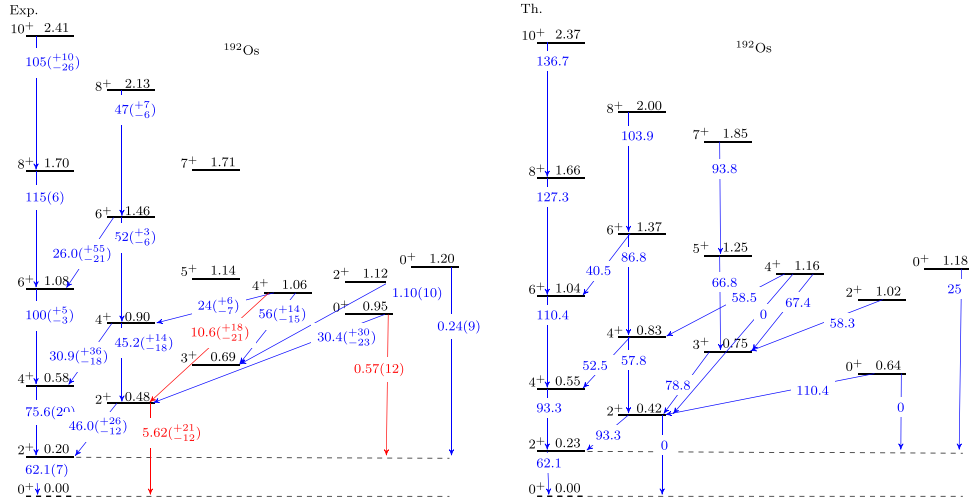

Figure 12. The same as figure 7 for ^{190}Os. The linear E2 operator, equation (15), has been used with $t = 9.53$ e b, in order to match the transition $B(E2; 2_1^+ \rightarrow 0_1^+)$. Four forbidden transitions with $B(E2) \leqslant 0.8$ W.u. were omitted for the sake of clarity. The two transitions indicated with green arrow occurs within the $(\xi, \tau) = (1, 3)$ multiplet and are forbidden due to the $\Delta\tau = 0$ selection rule.

Figure 13. The same as figure 7 for ^{192}Os. The linear E2 operator, equation (15), has been used with $t = 8.32$ e b, in order to match the transition $B(E2; 2_1^+ \to 0_1^+)$. Three forbidden transitions with $B(E2) \leqslant 0.41$ W.u. were omitted for the sake of clarity.

Table 5. Statistics of the experimentally observed $B(E2)$ values (in W.u.). Transitions between states that are assigned to model states are considered. The number and the mean $B(E2)$ values are displayed in the second and third column for transitions with $\Delta\tau = \pm 1$ allowed within the model. The same data are displayed in the fourth and fifth column for forbidden transitions (corresponding mainly to $\Delta\tau = \pm 2$), supplemented by the largest $B(E2)$ value, which is predicted to be zero in the model, as well as with the initial and final states of the corresponding transition. The three transitions within the same (ξ, τ) multiplet are not included.

Nucleus	Allowed E2 transitions		Forbidden E2 transitions				
	Number	$\langle B(E2)\rangle$	Number	$\langle B(E2)\rangle$	Largest $B(E2)$	L_i^π	L_f^π
^{188}Pt	5	133.0	0				
^{190}Pt	1	56.1	0				
^{192}Pt	6	77.5	2	0.62	0.68		
^{194}Pt	11	45.3	4	3.89	14.4	0_3^+	2_2^+
^{196}Pt	11	35.6	8	0.58	2.8		
^{198}Pt	6	32.0	3	0.23	0.60		
^{186}Os	13	87.6	7	3.0	9.4	2_2^+	0_1^+
^{188}Os	11	69.8	6	3.0	10.2	4_3^+	2_2^+
^{190}Os	16	59.3	7	2.46	7.3	4_3^+	2_2^+
^{192}Os	16	51.0	6	3.0	10.6	4_3^+	2_2^+

the present model the 4_3^+ and the 2_2^+ states are interpreted as model states with quantum numbers $(\xi, \tau) = (1, 4)$ and $(1, 2)$, so the $\Delta\tau = \pm 1$ selection rule forbids the E2 transition between them when using the β-linear operator, equation (15). This indicates, probably, a non-negligible mixing with other 4^+ and 2^+ states. In ^{186}Os the strongest theoretically forbidden transition is that from the 2_2^+ to the ground-state.

Another example is the transition from the $E_x = 1547$ keV 0^+ state to the 2_2^+ state in ^{194}Pt. This transition is comparable in strength to that to the 2_1^+ state (see also table 2). In the present approach this 0^+ state has been interpreted as the $(\xi, \tau) = (2, 0)$ bandhead state, which is not expected to decay to the 2_2^+ state with quantum numbers $(1, 2)$. The other 0^+ model state with quantum numbers $(1, 3)$ can decay to this state, however, it has been assigned to the first excited 0^+ state at $E_x = 1267$ keV on grounds of its decay pattern (see table 2). In the remaining Pt nuclei (^{192}Pt, ^{196}Pt and ^{198}Pt) the selection rules seem to be realized with better accuracy. It is notable that in many transitions with significant $B(E2)$ value that the model predicts to be forbidden, the 2_2^+ state appears as the initial or final state. This seems to indicate that this state has non-negligible mixing with other 2^+ states.

It is worthwhile to discuss transitions within the (ξ, τ) multiplets separately. These correspond to $\Delta \tau = 0$, and as such, they are forbidden if the linear $E2$ transition operator is used. It is found that only three such transitions occur, and only in ^{188}Os and ^{190}Os. The strongest one is $(1, 3)4^+$ to $(1, 3)3^+$ with $B(E2) = 54 + 24/ - 19$ W.u. in ^{190}Os. Such a strong transition within the $K^\pi = 2^+$ band would be characteristic of a rotational nucleus, indicating triaxial configuration. The two other examples $(1, 3)6^+$ to $(1, 3)4^+$ in ^{190}Os and $(1, 3)4^+$ to $(1, 3)6^+$ in ^{188}Os with $B(E2) = 6(4)$ and $15(6)$ W.u., respectively, are weaker and correspond to transitions between the $K^\pi = 2^+$ and the ground-state bands.

An overall observation regarding the $B(E2)$ values is that the model generally predicts stronger transitions than what is obtained from the experiment. It has to be mentioned here that the theoretical $B(E2)$ values are scaled by the requirement that the $B(E2; 2_1^+ \rightarrow 0_1^+)$ is reproduced. This may lead to a general overestimation of the transition strengths. However, the fact that the t parameter of the linear $E2$ transition operator (15) falls within a relatively narrow range may be considered as the sign of consistency. In-band transitions in the ground-state bands are generally reproduced well: with a few exceptions, the calculated $B(E2)$ values are close to the upper limit of the experimental data. Transitions within the $K^\pi = 2^+$ band are also reasonably reproduced: here the strength of transitions from the higher states tend to be overestimated. Interband transitions between the $K^\pi = 2^+$ and the ground-state band are typically also overestimated by a factor of two or three. Here there is a clear difference between the Pt and Os isotopes. According to the prediction of the model, the strength of the transitions to the 2_1^+ state from the 4_1^+ and 2_2^+ states is equal (this applies also to the $O(6)$ limit of the IBM). This expectation is fulfilled for the Pt isotopes, but it is not for the Os isotopes. In this case, the mean values of the former transition are several times stronger. The largest difference ($\sim$6 to 8) occurs on the light end of the isotope chain, and it gradually diminishes (to 3 and less than 2) for ^{190}Os and ^{192}Os (it may also be noted that the errors of the 2_2^+ to 2_1^+ transitions are comparable to the mean values, so the experimental ratios might be closer to the theoretical ones). This seems to indicate that the model performs better for the heavy Os isotopes, located near the closure of the $N = 126$ neutron shell. This finding seems to be confirmed by microscopic calculations. In [31] the structural evolution in neutron-rich Os and W isotopes was investigated using IBM and Hartree–Fock–Bogoliubov calculations with the Gogny-D1S energy density functional (EDF). It was found that the obtained energy surfaces for Os isotopes are rather flat in the γ degree of freedom: in fact, for ^{192}Os it was calculated to be γ-independent. Similar features can be seen in,[6] which displays plots concerning the deformation evolution of nuclei based on microscopic calculations. The lighter Os isotopes exhibit features close to a rotational character. Transitions from the excited 0^+ bandhead states and the 2^+ states built on them are also overestimated by the model in general. Here the

---

[6] https://wwwphynu.cea.fr/science_en_ligne/carte_potentiels_microscopiques/carte_potentiel_nucleaire_eng.htm.
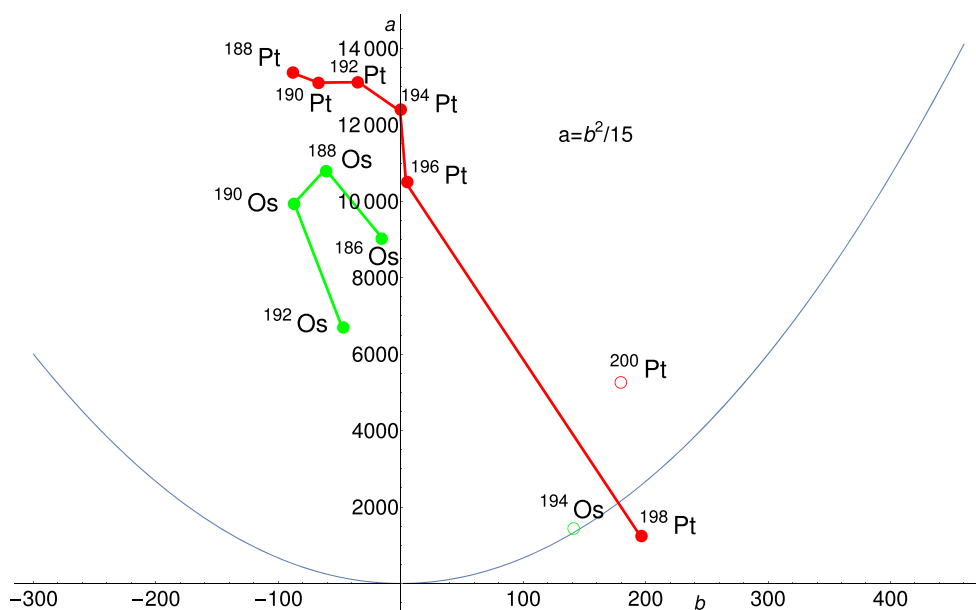
Figure 14. The location of the Pt and Os nuclei in the (a, b) phase space based on the fitted a and b parameter values. Open circles indicate the tentative position of the ^{200}Pt and ^{194}Os nuclei.

calculated values exceed the experimental ones by a factor of two to five. Generally, the results are rather similar to those obtained for the Ru and Pd isotopes [16].

It has to be noted that the $B(E2)$ values were calculated using the first-order transition operator (15). As it has been mentioned previously, the electric quadrupole moments calculated with this operator vanish. The experimentally known quadrupole moments of the 2_1^+ state are the following:[5] ^{192}Pt: $Q = +0.55(21)$ e b, ^{194}Pt: $Q = +0.48(14)$ e b, ^{196}Pt: $Q = +0.62(8)$ e b, ^{198}Pt: $Q = +0.42(12)$ e b, ^{186}Os: $Q = -1.63(4)$ e b, ^{188}Os: $Q = -1.46(4)$ e b, ^{190}Os: $Q = -1.18(3)$ e b, ^{192}Os: $Q = -0.96(3)$ e b. In summary, the ground-state configuration of the Pt isotopes has oblate shape, while that of the Os isotopes is prolate. The electric quadrupole momenta are non-zero, however, they are clearly smaller in magnitude that the corresponding values of the neighboring nuclei (W and Hf nuclei located closer to the mid-shell region typically have $Q \sim -2$ e b, while ^{184}Os has $Q = -2.7$ e b). A more realistic reproduction of the electric quadrupole momenta would be possible using the more general $E2$ operator (16) that includes a quadratic term too. This operator would also relax the selection rules by allowing transitions with $\Delta\tau = \pm 2$ and 0 too. However, we are not considering this option here.

As a summary of the present subsection, it may be noted that the performance of the sextic oscillator as a γ-independent potential in the Bohr Hamiltonian improves with increasing mass number in both chains. Indications for this are the trends in the splitting between even- and odd-spin levels in the $K^\pi = 2^+$ bands (for Pt nuclei) and the trends in the quality of fitting, D and in the ratios $B(E2; 4_1^+ \rightarrow 2_1^+)/B(E2; 2_2^+ \rightarrow 2_1^+)$ (for the Os nuclei). The lighter members of the chains, closer to the middle of the neutron shell might have influence from other shape configurations (e.g. rotational) too.
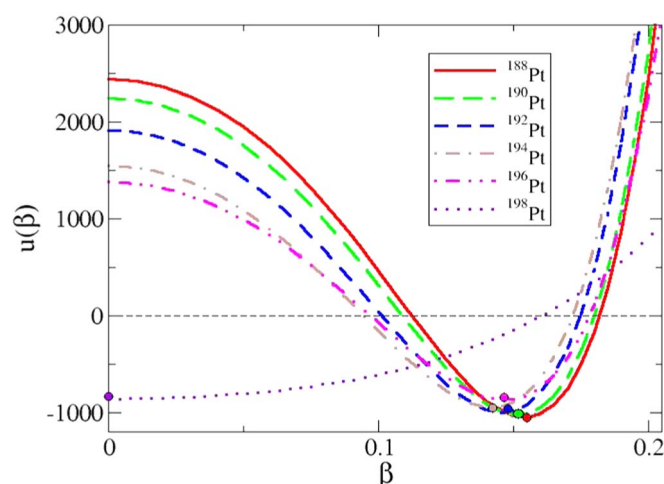
Figure 15. The potentials $u(\beta)$ calculated from the parameters a and b determined from the fitting procedure for Pt nuclei. The zero of the energy scale is chosen at the ground-state energy for all isotopes. Filled circles indicate the location of the potential minima.

3.3. Consequences regarding the phase space and potential shapes

Figure 14 displays the trajectory defined by the fitted a and b parameters in the (a,b) phase space for the Pt and Os isotopes. Most locations are above the critical parabola and close to the a-axis on its left, i.e. the b parameters are typically small and negative. This parameter combination corresponds to negative coefficients of the quadratic and quartic terms of the sextic oscillator potential (5). This leads to a potential with a deformed minimum ($|\beta| > 0$). The only exception is ^{198}Pt, which is located below the critical parabola, close to the b-axis with $b > 0$. For this parameter combination all three terms of the sextic oscillator have positive coefficients, leading to a spherical minimum ($\beta = 0$). Furthermore, the small a also means that this nucleus is close to the harmonic oscillator limit. These trajectories are different from those obtained for the Ru and Pd isotopes using the same model [16]. There the b parameter was found to be positive for each isotope, furthermore, most of the points were located below the critical parabola, corresponding to a spherical minimum. The Ru isotopes followed a trajectory from the right ($b \sim 300$) to the left ($b \sim 100$) as the mass number increased from $A = 98$ to 108, crossing the critical parabola near $A = 104$. The parameter b also decreased (from 300 to 200) for the Pd isotopes, as the mass number increased from 102 to 110, but the trajectory moved roughly parallel with the critical parabola, staying below it.

The potentials generated from the fitted parameter values a and b are displayed in figures 15 and 16. It is worth noting that for these γ-unstable systems the potential as a function of β is symmetric with respect to $\beta = 0$, that is for each nucleus minima of equal depth are found for $\pm|\beta|$ because the potential only contains even powers in β and it does not depend on the γ degree of freedom. This means that a prolate system with $\beta_0 > 0$ and $\gamma_0 = 0$ has the same energy as an oblate system with $\beta_0 > 0$ and $\gamma = \pi/3$. But this last situation is equivalent to $\beta = -\beta_0$ and $\gamma = 0$. Since we are not plotting γ, in figures 15 and 16 we include only positive β values, the figures are a projection of the energy surface on the $\gamma = 0$ plane for Pt isotopes (oblate shapes) and on the $\gamma = \pi/3$ for Os isotopes (prolate shapes). A symbol has been plotted in the actual minimum for each nucleus.
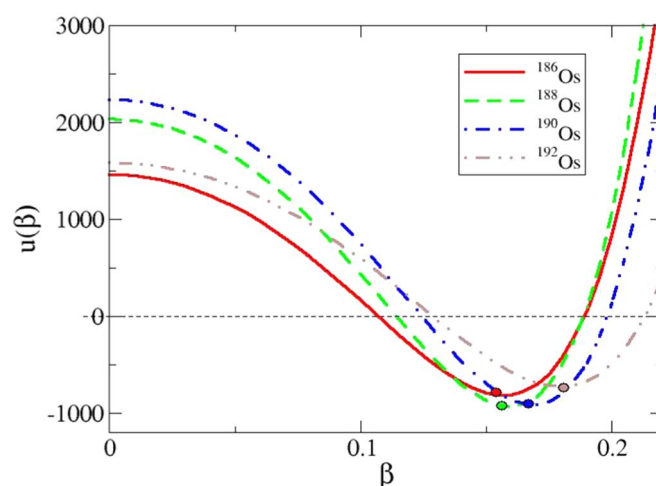
Figure 16. The same as figure 15 for the Os nuclei.

It is seen in figure 15 that the potential associated with ^{198}Pt differs from the other potentials in that it is the only one corresponding to a spherical minimum ($\beta_{min} = 0$). This is also the only example for which the first excited 0^+ state is interpreted as the $E_{2,0}$, rather than the $E_{1,3}$ theoretical level. All the rest of the Pt isotopes are calculated to be deformed with moderate β-deformations. The transition from the deformed minimum to the spherical one occurring in the Pt chain may be interpreted as the consequence of approaching the $N = 126$ closed neutron shell, where nuclei with the spherical (or U(5) in IBM) symmetry are expected (note that a similar trend was found in the Ru chain [16], which approaches the $N = 82$ shell closure for the light end of the chain). The investigation of ^{200}Pt is thus reasonable to decide the validity of this interpretation. For this, the properties of the first two 0^+ states and the E2 decays from them are crucial. There is a state with tentative 0^+ spin-parity assignment at 1118 keV and another one with firm 0^+ at 1583 keV, but there are no $B(E2)$ data available for ^{200}Pt. However, based on the findings on ^{198}Pt, one may expect that the first state is the model state with (2, 0) quantum numbers, while the second one is that with (1, 3). Considering heavier Pt isotopes, the energy spectrum of ^{200}Pt is far less well-known than those of the other Pt isotopes discussed here, so a parameter fit can be carried out only with fewer states. Applying the fitting procedure the ten lowest-lying positive-parity states one obtains $a = 5249$, $b = 179$ and $c = 11.5$. These values place this nucleus above the critical parabola in figure 14, i.e. into the domain with deformed potential minimum ($\beta > 0$). Most probably this is the consequence of the fact that the first excited 0^+ state is substantially higher (1118 keV) than the corresponding state in ^{198}Pt (914 keV).

Concerning Os, figure 16, all studied isotopes are calculated to be deformed (oblate, due to the know quadrupole moments) with moderate β-deformations. It should be worthwhile to investigate experimentally the next Os isotope too, i.e. ^{194}Os, to see whether the transition to the spherical domain can be observed. The indication for this would be the presence of two excited 0^+ states relatively low in energy. The spectrum of ^{192}Os is close to this arrangement (956 and 1206 keV). However, the corresponding states in ^{194}Os are located at 697 and 1540 keV, which is a rather different pattern. The possibility of an unobserved 0^+ state cannot be excluded, as most experimental states have tentative spin-parity assignment. There is a state, for example, at 1141 keV, which decays only into the 2_2^+ state. This state has a tentative spin-

parity assignment 4^+, however, it could also play the role of the $(1, 3)0^+$ model state, in which case the 697 keV state would correspond to the $(2, 0)0^+$ model state. This assumption is supported by the fact that this latter state decays to the 2_1^+ state. Accepting this assignment of the 0^+ states, it is possible to compose a relatively complete band structure of this nucleus: the members of the ground-state band and the $K^\pi = 2^+$ band can be identified from the experimental compilation up to $L^\pi = 8^+$ and 6^+, respectively. Altogether 13 experimental states can be assigned to model states based on their location and decay properties. A fit with these results in the parameter set $a = 1441$, $b = 144$ and $c = 5.2$. This places ^{194}Os almost right on the critical parabola in figure 14, just into the domain of deformed potential minimum. This calculation confirms tentatively that there is an emerging a shape phase transition on the heavy end of the Os isotope chain too, similarly to the Pt chain.

4. Summary and outlook

The sextic oscillator has been applied in the Bohr Hamiltonian to the chain of six Pt and four Os nuclei with the intention to explore a possible transition from the γ-unstable to the spherical vibrator shape phases. The theoretical model space contained 30 energy levels belonging to several bands, with L^π up to 10^+. The experimental states have been assigned to theoretical correspondents based on their location, the $B(E2)$ values of transitions they are involved in and their decay preferences (when no numerical data was available for their electromagnetic transitions). The assignment was essentially complete for the ground-state band and the $K^\pi = 2^+$ bands, while it was less complete for two excited $K^\pi = 0^+$ bands. The electric quadrupole transitions from the bandhead states of these $K^\pi = 0^+$ bands have been scrutinized in order to decide which one corresponds to a nodally excited configuration ($\xi = 2$). The order of these states is indicative of the equilibrium shape phase of the given nucleus. Typically there remained 5 to 10 unassigned theoretical states usually above 2000 keV excitation energy, where the experimental data set tends to be incomplete (from the theoretical side, these states represent nodal excitations, i.e. $\xi = 2$ or 3).

The potential parameters have been extracted from a two-step fitting procedure, and the theoretical energy spectra have been determined for each nucleus. For the Os isotopes the quality of the fit was similar to that obtained in a previous application of the model to Ru and Pd nuclei [16], while it was better for the Pt isotopes. From the more than 200 levels fitted, there were 13 for which the energy difference of the observed and calculated energy exceeded 200 keV.

The ground-state bands were reproduced with rather good accuracy, while for the $K^\pi = 2^+$ bands the splitting between the neighbouring even- and odd-spin levels was not always reproduced. An important and systematic trend has been identified for the two excited $K^\pi = 0^+$ bands. The members of the one with no nodal excitation ($\xi = 1$) exhibited a nearly constant (Os chain) or slowly increasing (Pt chain) trend with increasing mass number, while the members of the nodally excited band ($\xi = 2$) moved rapidly (Pt chain) or less rapidly (Os chain) to lower energies. As a result, the nodally excited configuration got below the nodally not excited one for the heaviest Pt isotope (^{198}Pt), while this situation was nearly reached for the heaviest Os isotope (^{192}Os). This trend was tentatively supported by the analysis of the next members of both chains (^{200}Pt and ^{194}Os), although the experimental data is far less complete for these nuclei. This means that there may be an emerging phase transition from the γ-unstable to the spherical vibrator shape as the mass number is increasing.

The analysis of the electric quadrupole transitions showed that the available $B(E2)$ values are reproduced rather well for in-band transitions in the ground and $K^\pi = 2^+$ bands, while the strength of interband transitions between these two bands are overestimated. An interesting exception for

this occurs for the Pt isotopes: there the strength of the transition from the 4_1^+ and the 2_2^+ states to the 2_1^+ state is equal, in accordance with the experiment (and also in line with the $O(6)$ limit of the IBM). Electric quadrupole transition from the excited $K^\pi = 0^+$ bands are also overestimated by the model, but the general trends on the forbidennes are consistently reproduced.

In the calculations, the first-order electric quadrupole transition operator has been used, which predicts the $\Delta\tau = \pm 1$ selection rule for the seniority quantum number τ. This is generally in accordance with the experimental data, as most of the theoretically forbidden transitions have small $B(E2)$. The few exceptions are transitions in which the 2_2^+ states are involved, indicating that there may be a mixing of the 2^+ states. The same operator and selection rule predicts vanishing quadrupole moments for the 2_1^+ states. However, the observed quadrupole moments in these isotopes are typically in the range $Q \sim +0.5$ to 1 e b for the Pt isotopes and $Q \sim -1$ to 1.5 e b for the Os nuclei, i.e. they are moderate, but non-zero. It may be noted that the $\Delta\tau = \pm 1$ selection rule of the linear $E2$ operator is the consequence of the tensorial character of the basis and the operators, and occurs in any model using the $O(5) \supset O(3)$ basis. More relaxed selection rules and non-zero electric quadrupole moments could be obtained by including a second-order term in the transition operator.

In summary, the model gives a reasonable description of the Pt isotopes as γ-unstable nuclei, while its performance is less accurate for the Os nuclei (especially the lighter ones), which seem to exhibit also rotational features, characteristic of a triaxial configuration. These findings are in line with a study performed for the same nuclei within the framework of the Interacting Boson Model [32].

Based on the results of the present study, the applications of the model to further isotope chains seems possible and desirable. The investigation of the Te, Xe and Ba isotope chains would be natural candidates. These nuclei are located above the closure of the $Z = 50$ proton shell and near the closure of the $N = 82$ neutron shell, and have been identified as good candidates for $E(5)$ symmetry [33].

Acknowledgments

Data availability statement

All data that support the findings of this study are included within the article (and any supplementary files).

ORCID iDs

S Baid ⬤ https://orcid.org/0000-0002-6757-6042
G Lévai ⬤ https://orcid.org/0000-0003-3785-3165
J M Arias ⬤ https://orcid.org/0000-0001-7363-4328

References

[1] Bohr A 1952 *Mat. Fys. Medd. Dan. Vid. Selsk.* **26** 14
[2] Bohr A and Mottelson B R 1953 *Mat. Fys. Medd. Dan. Vid. Selsk.* **27** 16
[3] Bohr A and Mottelson B 1975 *Nuclear Structure* vol 2 (Reading, MA: Benjamin)
[4] Iachello F and Arima A 1987 *The Interacting Boson Mode* (Cambridge: Cambridge University Press)
[5] Ginocchio J N and Kirson M W 1980 *Phys. Rev. Lett.* **44** 1744
[6] Ginocchio J N and Kirson M W 1980 *Nucl. Phys.* A **350** 31
[7] Dieperink A E L, Scholten O and Iachello F 1980 *Phys. Rev. Lett.* **44** 1747
[8] Iachello F 2000 *Phys. Rev. Lett.* **85** 3580
[9] Iachello F 2001 *Phys. Rev. Lett.* **87** 052502
[10] Cejnar P and Julie J 2009 *Prog. Part. Nucl. Phys.* **62** 210
[11] Fortunato L 2005 *Eur. Phys. J.* A **26** 1
[12] Lévai G and Arias J M 2004 *Phys. Rev.* C **69** 014304
[13] Ushveridze A G 1994 *Quasi-Exactly Solvable Models in Quantum Mechanics* (Bristol, UK: Institute of Physics Publishing)
[14] Turbiner A V 2016 *Phys. Rep.* **642** 1
[15] Lévai G and Arias J M 2010 *Phys. Rev.* C **81** 044304
[16] Lévai G and Arias J M 2021 *J. Phys. G: Nucl. Part. Phys.* **48** 085102
[17] Raduta A A and Buganu P 2011 *Phys. Rev.* C **83** 034313
[18] Raduta A A and Buganu P 2013 *J. Phys.* G **40** 025108
[19] Buganu P and Budaca R 2015 *Phys. Rev.* C **91** 014306
[20] Buganu P and Budaca R 2015 *J. Phys.* G **42** 105106
[21] Budaca R, Buganu P, Chabab M, Lahbas A and Oulne M 2016 *Ann. Phys. (N.Y.)* **375** 65
[22] Budaca R, Budaca A I and Buganu P 2019 *J. Phys. G: Nucl. Part. Phys.* **46** 125101
[23] Lahbas A, Buganu P and Budaca R 2020 *Mod. Phys. Lett.* A **35** 2050085
[24] Cizewsi J A, Casten R F, Smith G J, Stelts M L, Kane W R, Börner H G and Davidson W F 1978 *Phys. Rev. Lett.* **40** 167
[25] Baid S, Lahbas A and Oulne M 2022 *J. Phys. G: Nucl. Part. Phys.* **49** 045101
[26] Buganu P *et al* 2018 *Nucl. Phys.* A **970** 272
[27] Budaca A I and Budaca R 2017 *Phys. Scr.* **92** 084001
[28] El Korchi S A, Baid S, Buganu P, Chabab M, El Batoul A and Lahbas A 2022 *Nucl. Phys.* A **1017** 122354
[29] Ishkhanyan A M and Lévai G 2020 *Phys. Scr.* **95** 085202
[30] Wilets L and Jeans M 1956 *Phys. Rev.* **102** 788
[31] Nomura K, Otsuka T, Rodríguez-Guzmán R, Robledo L M, Sarriguren P, Regan P H, Stevenson P D and Podolyák Z 2011 *Phys. Rev.* C **83** 054303
[32] Bijker R, Dieperink A E L and Scholten O 1980 *Nucl. Phys.* A **344** 207
[33] Clark R M *et al* 2004 *Phys. Rev.* C **69** 064322